Supporting Information

Bacterially synthesized ferrite nanoparticles for magnetic hyperthermia applications

E. Céspedes,* J. M. Byrne, N. Farrow, S. Moise, V. S. Coker, M. Bencsik, J. R. Lloyd and N. D. Telling

1. AC susceptibility simulations

a) Details of model – clusters of polydisperse nanoparticles

The complex AC susceptibility (χ) of a magnetic particle suspension, $\chi = \chi' - i\chi''$, can be described within the linear response theory as discussed in detail elsewhere.[i,ii,iii] In order to model the AC susceptibility we considered clusters formed from aggregated nanoparticles, similar to that observed experimentally (as discussed in the main paper). The real and imaginary components of the AC susceptibility of the j^{th} particle within the i^{th} host cluster can be written as

$$\chi'_{ij} = \frac{1}{1+\phi_{ij}^2}\chi_{ij}^0 \quad (1)$$

$$\chi''_{ij} = \frac{\phi_{ij}}{1+\phi_{ij}^2}\chi_{ij}^0 \quad (2)$$

where the constant χ_{ij}^0 is given by $\chi_{ij}^0 = \mu_0 M_S^2 V_{ij}/3k_B T$ (where M_S is the saturation magnetization per unit volume, T is temperature, V_{ij} is the *particle* volume and other terms have their usual meaning); and $\phi_{ij} = \omega\, t_{ij}^{eff}$ where ω is the angular frequency ($\omega = 2\pi f$). The effective relaxation time of each particle in the cluster depends on the Néel relaxation time of the *particle*, t_{ij}^N and the Brown relaxation time of the host *cluster*, t_i^B according to $t_{ij}^{eff} = t_{ij}^N\, t_i^B/\left(t_{ij}^N + t_i^B\right)$ where the usual expressions are given for

$$t_{ij}^N = t_0 exp\left(\frac{KV_{ij}}{k_B T}\right) \quad (3)$$

$$t_i^B = \frac{\pi\eta D_i^3}{2k_B T} \quad (4)$$

and t_0=10^{-9} s, K is the particle magnetic anisotropy, η is the viscosity of the nanoparticle suspension and D_i is the diameter of the host cluster (i.e. the hydrodynamic size of the cluster).

The susceptibility of each cluster is given by the sum of the susceptibilities of each particle within the host cluster, using equations (1)-(4) given above. The real and imaginary components of the total susceptibility for the nanoparticle suspension (neglecting any minor contribution from the suspension medium) are thus given simply by

$$\chi' = \sum_i \sum_j \frac{1}{1+\phi_{ij}^2}\chi_{ij}^0 \quad (5)$$

$$\chi'' = \sum_i \sum_j \frac{\phi_{ij}}{1+\phi_{ij}^2}\chi_{ij}^0 \quad (6)$$

This approach also assumes that the clusters are relatively loosely packed such that particle-particle magnetic interactions can be neglected.

The way in which each particle dictates the susceptibility of the cluster as a whole is best illustrated by considering two specific cases at the same fixed temperature, as shown in **Figure S1**.

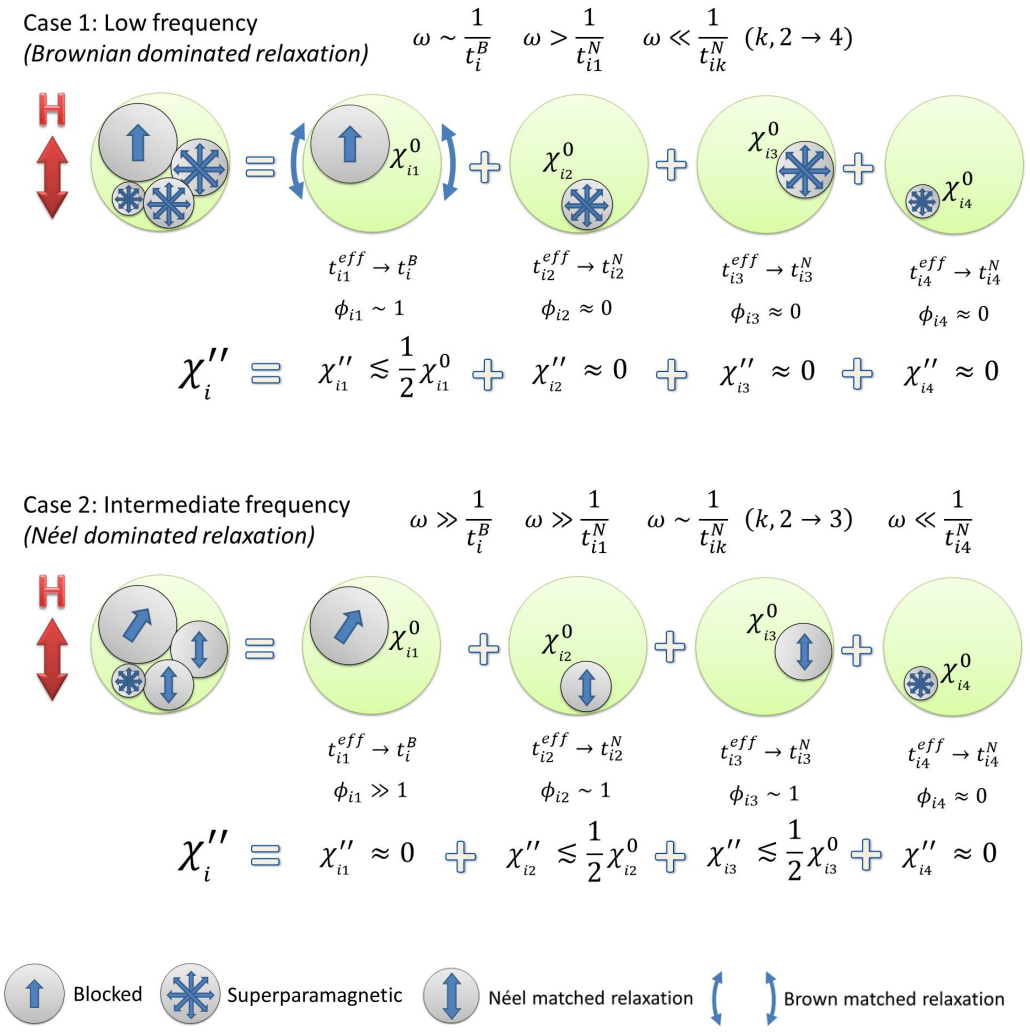

Figure S1. (color on-line) Schematic showing the modelled behavior of a mixed population of blocked and superparamagnetic particles within a typical host cluster (aggregate), for two specific frequencies of applied magnetic field.

At an applied field frequency matched to the Brown relaxation time of the cluster (Case 1), the susceptibility will be equal to the sum of the susceptibilities of blocked particles in the cluster, with the ϕ_{ij} term in equations (1) and (2) determined by t_i^B. At this frequency, superparamagnetic particles will not contribute and the susceptibility will depend on the diameter of the cluster and the viscosity of the suspension medium (as dictated by eqn. 4). In contrast, at higher frequencies (Case 2) the susceptibility will depend only on particles whose Néel relaxation times are matched to the applied frequency, and will therefore be insensitive to the size of the cluster. Thus, assuming all particles have the same anisotropy constant, the susceptibility of the suspension will depend on the distribution of particle sizes within clusters, in addition to the distribution of the cluster sizes themselves.

b) Generation of model nanoparticle clusters

In order to compute the overall AC susceptibility from a nanoparticle suspension using equations 1-6, it was first necessary to create a realistic model population of nanoparticle clusters. This was done by generating an ideal log-normal distribution of cluster diameters, and filling these clusters with particles selected at random from a log-normal distribution of particle diameters. Particles were added to the clusters until the effective cluster diameter was approximately equal to the ideal diameter. For computational ease the population was limited to 10,000 clusters.

A simple algorithm was used to generate the nanoparticle clusters for the model. For each cluster diameter in the log-normal distribution generated by input parameters, spherical nanoparticles were selected at random from a further log-normal distribution of particles. The total volume of this group of nanoparticles was calculated and compared to the volume of the idealized (spherical) cluster with diameter D_{in}. Further nanoparticles were randomly selected until the next selected particle caused the equivalent sphere volume to overshoot the ideal cluster volume by more than 10%. This particle was discarded and the remaining particles were used for the output (spherical) cluster with an effective diameter D_{out}. The process is illustrated schematically in **Figure S2**.

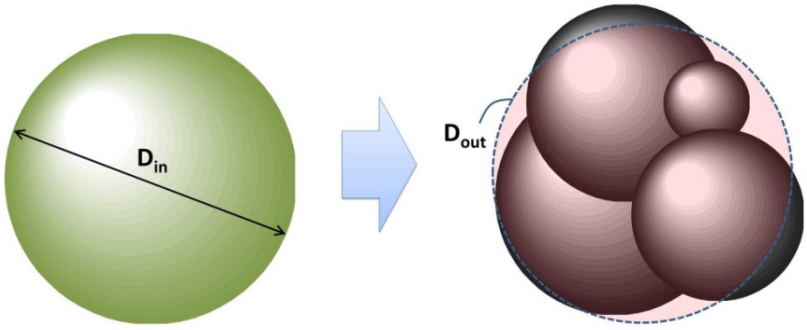

D_{in} (nm)	Particle diameters (nm)				D_{out} (nm)
33.4	22.7	27.2	9.9	19.8	34.4

Figure S2: Schematic showing the generation of nanoparticle clusters for ac susceptibility simulations.

The comparison between the idealized (input) log-normal distribution of cluster diameters (D_{in}) and the distribution of actual (output) cluster diameters (D_{out}), used for the AC susceptibility simulations in the main paper, is given in **Table S1**. Only a subtle increase in the mean cluster size and dispersive index is found in most cases, evidencing a generally good agreement between the actual and idealized values, and also between the modelled and measured parameters (from **Table 1**, main paper). Some examples of both ideal (input) and

actual (output) distributions are shown in **Figure S3**, evidencing good fitting of the output cluster values to log-normal distributions.

Table S1. Summary of cluster distribution parameters (idealized (input) and actual (output) values) from AC susceptibility simulations of the samples summarized in Table 1 (main paper).

Sample label	Idealized		Actual	
	D_H (nm)	$\sigma_{(DH)}$	D_H (nm)	$\sigma_{(DH)}$
MN_A	48	0.28	49	0.29
MN_B	70	0.30	72	0.30
$Co_{0.4}$	23	0.32	23	0.36
$Co_{0.7}$	22	0.31	22	0.31
$Zn_{0.2}$	28	0.29	28	0.32
$Zn_{0.4}$	43	0.29	44	0.29

The similarity of the distribution of final cluster diameters compared to the ideal log-normal distribution depends on the parameters of the log-normal distributions of both clusters and particles employed. However, for most experimentally relevant cases a reasonable agreement is obtained, and the final cluster population gives a good representation of a real polydisperse nanoparticle suspension. In the main paper, the values reported for the mean and dispersive index of the cluster distributions are determined from subsequent log-normal fits to the actual populations created by the model, rather than simply the idealized starting parameters.

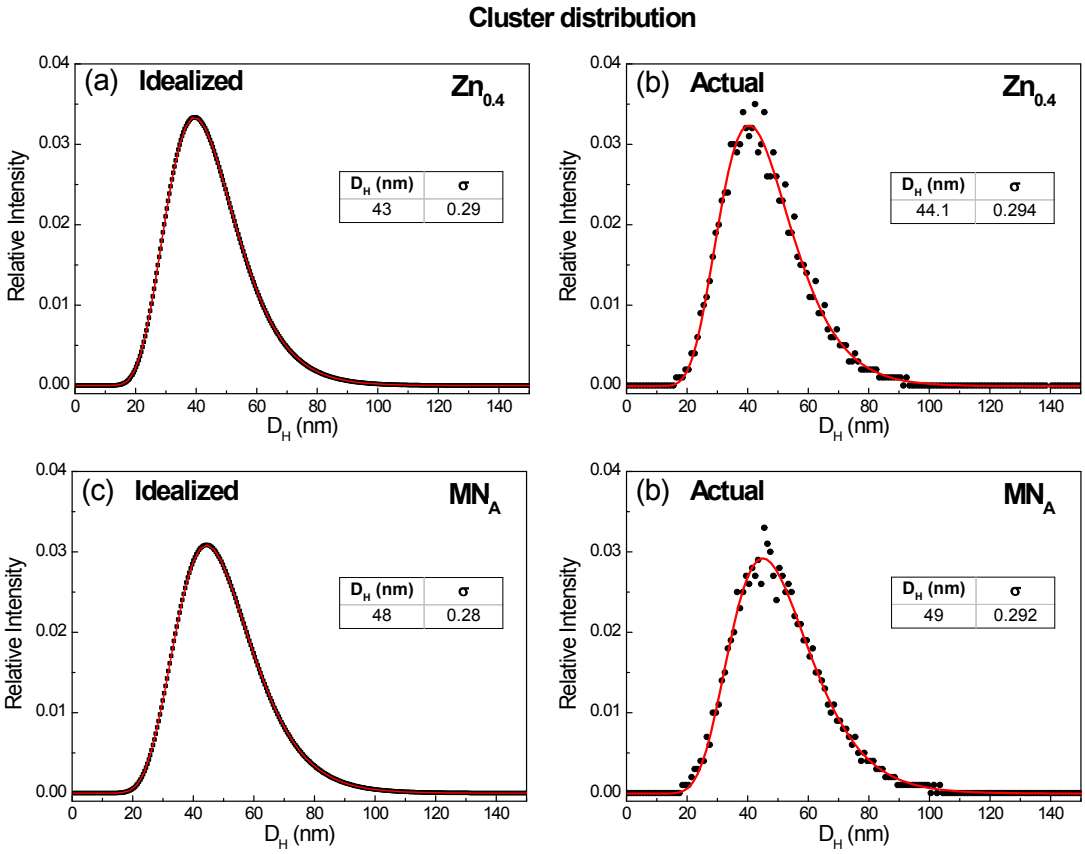

Figure S3. Comparison between idealized (input) log-normal cluster distribution and the actual (output) generated in the model, for two representative samples.

Another advantage of performing simulations based on a modelled nanoparticle population, compared to other calculations that consider distributions of both the nanoparticle and hydrodynamic sizes (see for e.g. Chung et al.[iv]), is that additional size dependent factors can be easily included. For example particle size dependent saturation magnetization, $M_{S_{ij}}$ and anisotropy, K_{ij} terms can be substituted into equations (1)-(3). For simplicity, in the results discussed here we have used constant values of M_S and K in the simulations.

2. Heating Curves and Specific Absorption Rate (SAR) Determination

Examples of the experimental heating curves per mass of iron for all the investigated samples at a selected frequency of 87 kHz and magnetic field amplitude of 20 mT are shown in **Figure S4**. **Figures S4 (a)** and **(c)** display the temperature rise versus time for the undoped and Co and Zn-doped nanoparticles in water, where the largest SAR values have been found (reported in **Tables 2** and **3**. **Figures S4 (b)** and **(c)** summarizes the heating effect for those nanoparticles in glycerol, showing a considerably reduced hyperthermia effect since only Néel and hysteresis mechanisms are possible for immobilized particles. The SAR was calculated from the initial linear rise in temperature versus time, normalized to the mass of iron (plain lines in **Figure S4**) and multiplied by the heat capacity of the sample. Measured samples showed an initial linear heating regime typically in 0-100 seconds.

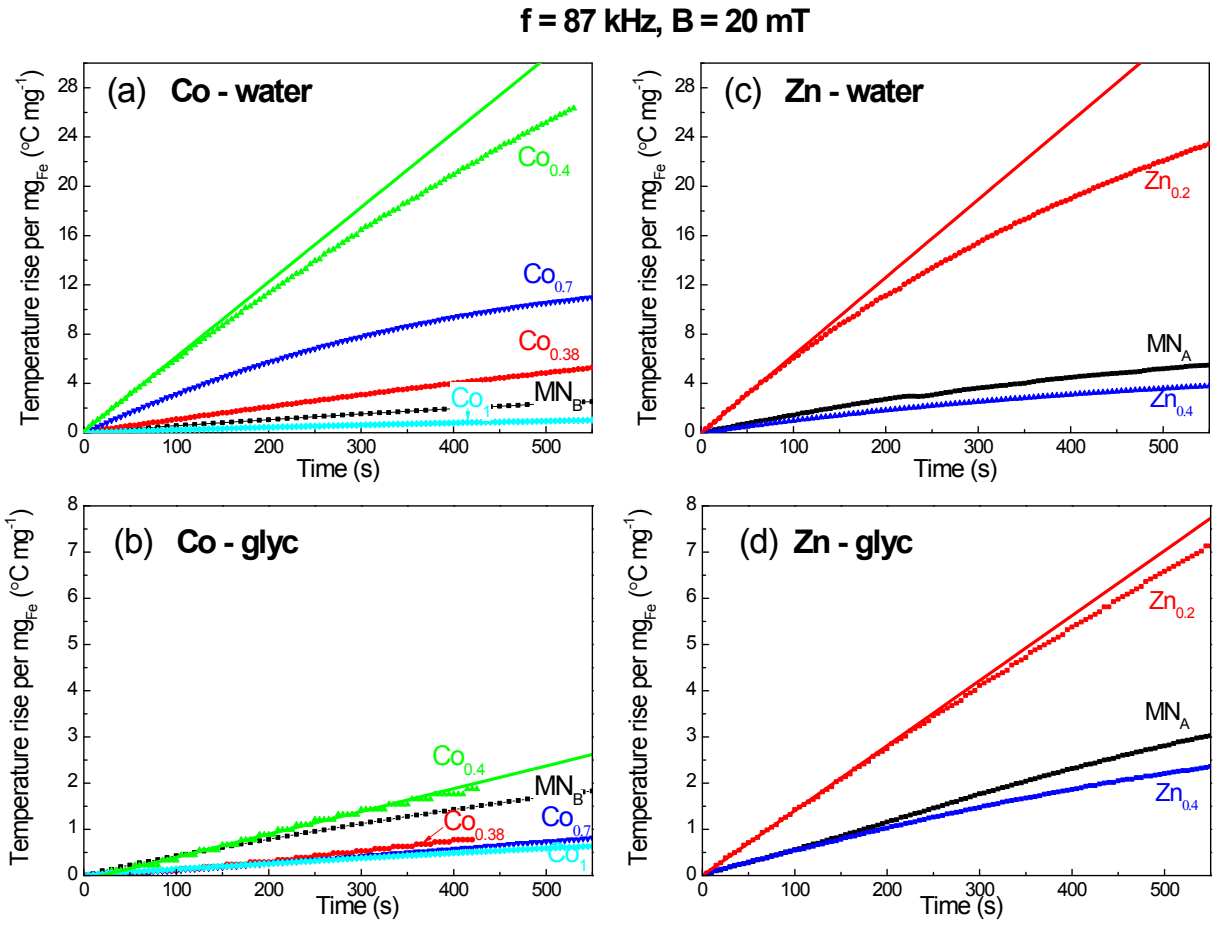

Figure S4. (color on-line) Increase in temperature per mass of iron for the undoped and Co and Zn-doped NPs solutions suspended in water, (a) and (c), and in glycerol, (b) and (d), under an AC magnetic field of 87 kHz and 20 mT. Solid lines (displayed just for the samples showing the largest heating in each case) correspond to the linear fit used to determine the SAR values reported in **Tables 2** and **3** (main paper).

SAR values from Tables 2 and 3 of the main manuscript (measured at the maximum available magnetic field at each frequency) have been normalized to H^2f for a better comparison of the heating efficiency among all samples (Fig. S5). Maximum values in water appear for $Zn_{0.2}$ and $Co_{0.4}$ at the lowest available frequency (87 kHz). As expected, a notable decrease is observed in glycerol, reaching the largest normalized values for the $Zn_{0.2}$ sample at the lowest frequencies, with higher values recorded for MN_B at larger frequencies.

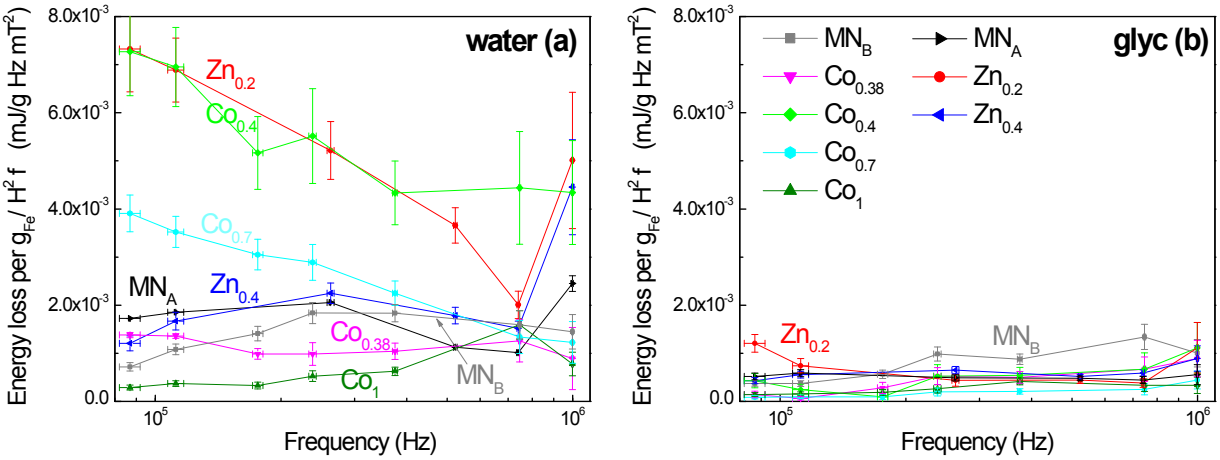

Figure S5. (color on-line) Energy loss per mass of iron during magnetic hyperthermia (from SAR values) normalized to H^2 and frequency in order to compare all the measured samples under different conditions (magnetic field amplitude and frequency) in water (a) and glycerol (b).

3. AC susceptibility simulations and relaxation/heating mechanisms

The simulated susceptibility spectra generated across a broad frequency range are displayed in **Figure S6** for (a) MN_A, (b) $Zn_{0.2}$ and (c) $Zn_{0.4}$, which show mixed relaxation mechanisms due to populations consisting of blocked and SPM MNPs, dependent on anisotropy. Simulations have been performed for MNPs in water, glycerol, and using a hypothetical high viscous solvent (to ensure immobilization of the MNPs) to completely isolate the Néel contribution from the Brown relaxation. Accordingly, both Brown relaxation (dependent on the fluid viscosity) and Néel relaxation (appearing at fixed frequency) can be distinguished in the simulated susceptibility spectra. The complete match above 1 kHz between the susceptibility spectra for NPs in glycerol, and fully immobilized NPs ($\eta >>$), for all samples, demonstrates the total immobilization of the NPs in glycerol at the frequency range used for magnetic hyperthermia (87 kHz to 1 MHz).

Further details of the mixed relaxation mechanisms in the Zn-doped samples can be observed in **Figure S7**, which shows the comparison of the different χ'' contributions from the simulated data for the NPs in water (**Figure S7a**) and glycerol **(Figure S7b)**. According to their relative proportion of blocked particles, in water mixed relaxation processes ranging from largely Brown ($Zn_{0.2}$), intermediate (MN_A) and predominantly Néel ($Zn_{0.4}$) relaxation, are found. This can be seen from the varying intensity of the Brown relaxation peaks for each sample (**Figure S7a**). Considering the specific frequency range of magnetic hyperthermia measurements (between dotted lines in the figure), the SAR trend found for these samples (see **Table 3** and **Figure 6**, main paper) appears compatible with their simulated χ'' behaviour. In particular, comparing the three χ'' curves in water, considerably larger SAR values at low frequency (87 kHz) emerging from Brown relaxation would be expected for $Zn_{0.2}$ with respect to $Zn_{0.4}$ and MN_A. However such differences are less significant at the largest frequency (1MHz), where comparable SAR values were found for $Zn_{0.2}$ and $Zn_{0.4}$, as expected due to their more similar χ'' intensities at this frequency.

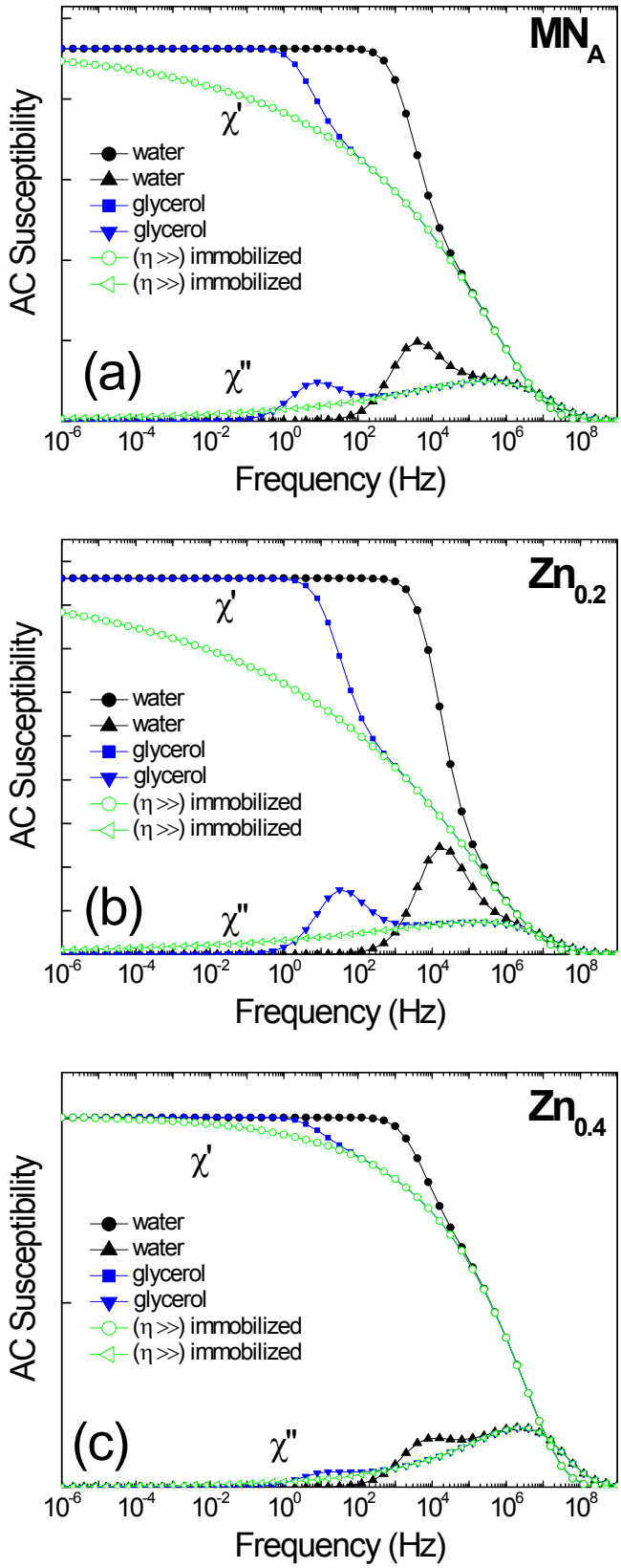

Figure S6. (color on-line) Simulation of AC susceptibility spectra including regions below and above the experimental frequency range for (a) MNA, (b) $Zn_{0.2}$ and (c) $Zn_{0.4}$ nanoparticles suspended in water, glycerol and a hypothetical high viscous solvent ($\eta \sim 10^{18}$ Pas; to completely immobilize NPs).

When suspended in glycerol, Néel based processes become significant at the frequencies of interest for hyperthermia treatments (see **Figure S7b**). In this case the enhancement of the χ'' curve for $Zn_{0.4}$ compared to $Zn_{0.2}$ is consistent with the higher SAR values measured in $Zn_{0.4}$ for frequencies over 200 kHz. Nonetheless, a simple direct extrapolation from susceptibility data to SAR is not possible. Whilst AC susceptibility is measured at small field amplitudes, considerably larger fields are used for hyperthermia (up to 20 mT for the lowest frequency of 87 kHz). At these fields magnetic heating arising from nonlinear ferromagnetic hysteresis losses has to be considered.

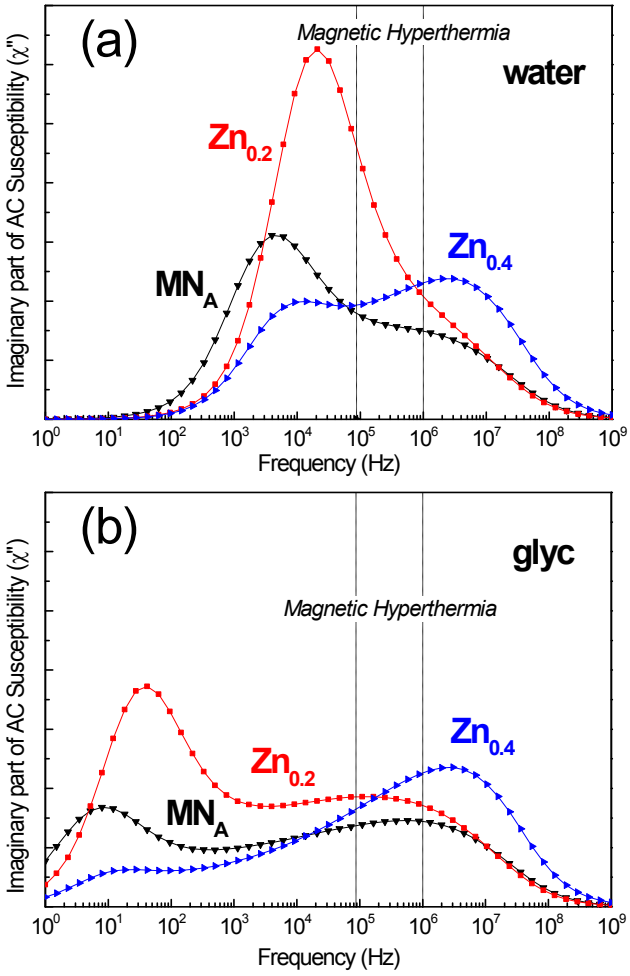

Figure S7. (color on-line) Comparison among the simulated χ" susceptibility of MN_A, $Zn_{0.2}$ and $Zn_{0.4}$ nanoparticles (a) in water and (b) in glycerol (using simulation parameters summarized in Table 1, main paper). Dotted lines show the lowest and highest frequencies used for magnetic hyperthermia, 87 kHz and 998 kHz, respectively.

[i] R.E. Rosensweig, *J. Magn. Magn. Mater.* **2002**, 252, 370–374.
[ii] R. Hergt, S. Dutz, M. Zeisberger, Nanotechnology **2010**, 21, 015706.
[iii] M. Shliomis, Sov. Phys. Uspekhi (Engl. transl.) **1974** 17, 153.
[iv] S.-H. Chung, A. Hoffmann, K. Guslienko, S. D. Bader, C. Liu, B. Kay, L. Makowski, L. J. Chen, J. Appl. Phys. **2005**, 97, 10R101.